

# Nanoscale heterogeneities drives enhanced binding and anomalous diffusion of nanoparticles in model biomembranes: Supplementary information

Roobala Chelladurai,<sup>†</sup> Koushik Debnath,<sup>‡</sup> Nikhil R. Jana,<sup>‡</sup> and Jaydeep Kumar  
Basu<sup>\*,†</sup>

<sup>†</sup>*Department of Physics, Indian Institute of Science, Bangalore 560012, India*

<sup>‡</sup>*Centre for Advanced Materials, Indian Association for the Cultivation of Sciences,  
Kolkata 700032, India*

E-mail: basu@physics.iisc.ernet.in

Phone: 080 2293 3281

## Sample details

### Preparation of supported lipid bilayer

Langmuir Blodgett technique is used widely in preparing model cell membranes and known for preparing asymmetric bilayers, tune the packing etc. Bilayers used in this study were prepared on RCA (3:1 mixture of  $NH_4OH$  and  $H_2O_2$ ) cleaned cover glass (0.17mm thickness, 20 x 20 mm from Glaswarenfabrik KARL HECHT GmbH &Co KG). Bilayers were transferred at an optimal pressure and temperature of 32 mN/m and 15°C. At this temperature, we could transfer defect free layers and this pressure is used by different groups for its sig-

nificance of *monolayer – bilayer equivalence pressure*.<sup>1</sup> Corresponding pressure - area isotherm is shown in Figure S1. Transferred bilayer were always stored under water and used for experiments shortly after preparation.

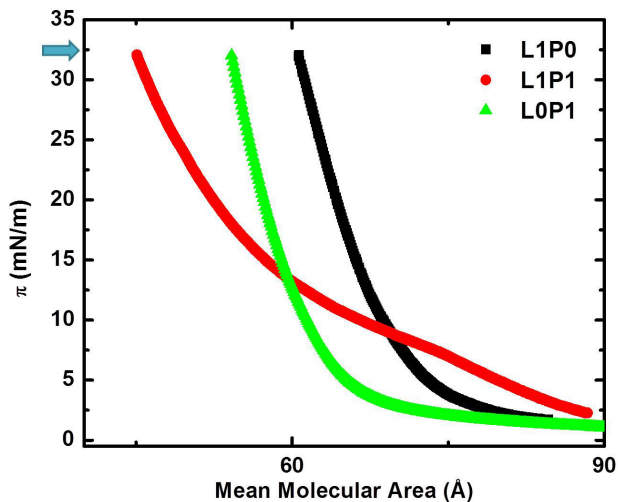


Figure S1: LB compression cycle for different compositions of L1P0 and L0P1. Arrow marked in the figure indicates the pressure at which bilayers are transferred.

## Characterization of QD

We have characterized the size distribution of QD using TEM and DLS measurements as shown in Figure S2. QDs in final form is hydrophilic in nature and highly water soluble. They are positively charged with a net charge of + 20 at pH 7.4. These QDs are red emissive and corresponding excitation spectra is given in Figure S2 (b).

## Fitting FCS data

### Bilayer Characterization

One of the important physical parameters that quantify the phase properties of bilayers is, lipid diffusion. FCS measurements are routinely used in extracting the time scales of diffusion in bilayers. For lipids diffusing in a 2D planar membrane, decay of intensity -

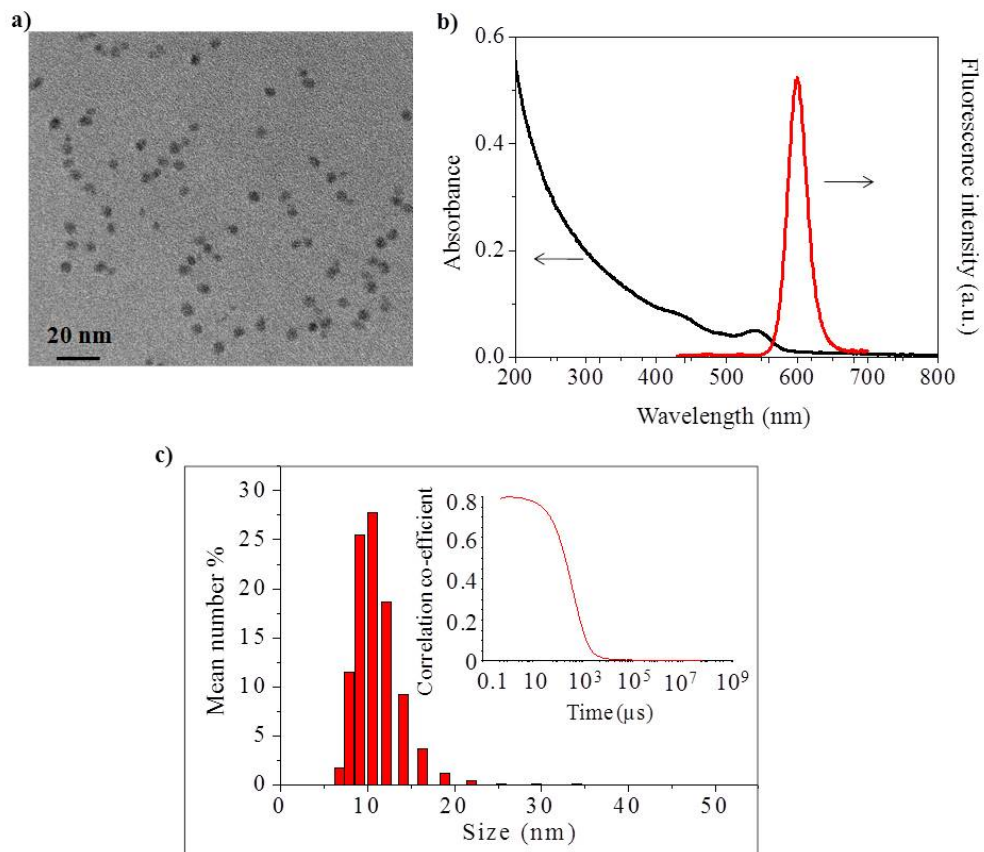


Figure S2: a) TEM image, b) absorption and fluorescence spectra and c) dynamic light scattering-based hydrodynamic size distribution (along with correlation co-efficient at inset) of polyacrylate coated QD.

intensity correlation is fit using a function given by,

$$G(t) = \frac{G(0)}{1 + \frac{t}{\tau_d}}, \quad (1)$$

where  $G(0)$  - amplitude of the correlation,  $\tau_d$  - transit time extracted by fitting the data. Figure S3 shows the fitting of auto correlation functions measured at different times on a DLPC bilayer after addition of QD. In the main text, we have shown in Figure 2a, that effect of QD fluidize the membrane, and Figure 2d shows continuous decrease in intensity measured from the membrane plane indicating drop in lipid density. Correlation curves shown in Figure S3 also shows increase in  $G(0)$  with time indicating drop in number density of lipids with time and subsequent fluidization effect. Figure 3b shows changes in  $G(0)$  that reflects on the lipid density / number ( $N$ ) as  $G(0) \sim \frac{1}{N}$ .

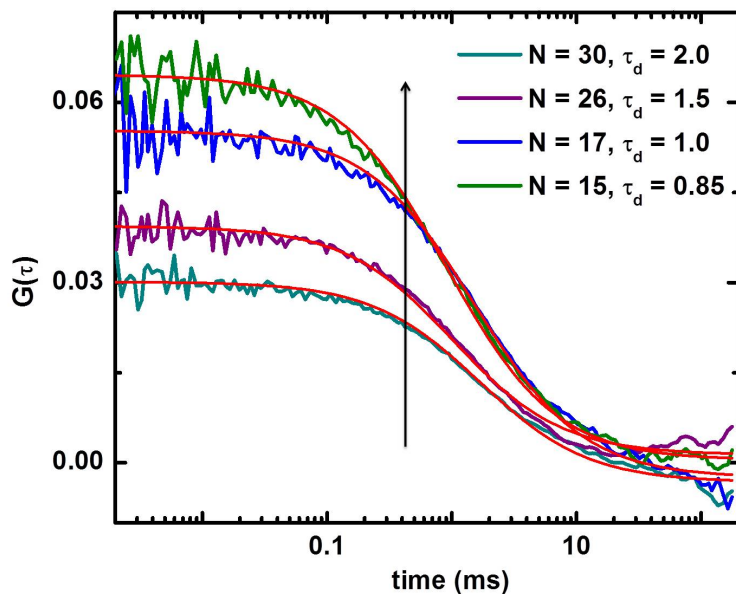


Figure S3: Unnormalized autocorrelation FCS data measured on a DLPC bilayer after QD addition measured at different times. Single component 2D fit done on correlation data collected from DLPC after QD addition. Arrow mark indicates the increase in amplitude of correlation due to reduction in lipid density on QD addition .

## QD diffusion

QDs in water / PBS buffer exhibits very fast kinetics and the corresponding correlation curve of a typical data is shown in Figure S4. Using a 3D model (Eqn 2), we obtained a time scale of 0.7 ms.

$$G(t) = \frac{G(0)}{1 + \frac{t}{\tau_d}} \cdot \frac{1}{1 + \left(\frac{t}{\tau_d \kappa^2}\right)}, \quad (2)$$

where the second factor comes due to the axial extension of the laser beam and  $\kappa = \frac{z}{w}$ ,  $z$  &  $w$  corresponds to axial and lateral dimensions of the beam.  $\kappa$  is the structure factor of the beam and usually comes in the range of 5 - 6.

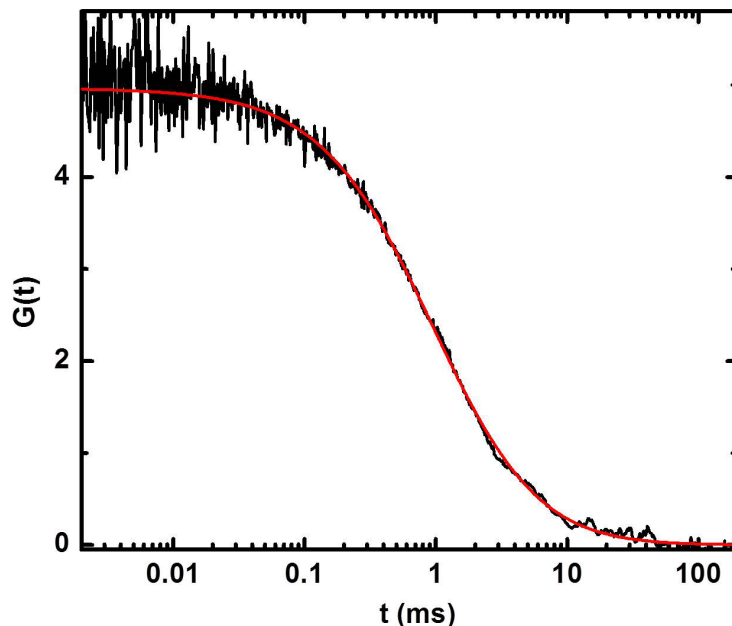


Figure S4: FCS correlation curve measured in bulk from QD diffusion

After adding QDs to this system, they start to bind onto the membrane and starts to exhibit slow diffusion as they are now restricted to move in a viscous medium (lipid bilayer). Unlike in lipid case, QD data could not be fit using Eqn 1 as shown in Figure S5. QD correlation data and fitting done using 1 component and 2 component model are shown in Figure S5. For a general 'i' component, correlation function is given by,

$$G(t) = \sum_i G^i(0) (1 - T + T \exp \frac{-t}{\tau_T}) (\frac{1}{1 + (\frac{t}{\tau_{d,i}})^{\alpha_i}})^{-1}, \quad (3)$$

with index for different components  $i$ , correlation function  $G(t)$ , amplitude  $G(0)$ , correlation time  $t$ , triplet fraction  $T$ , triplet time  $\tau_T$ , transit time  $\tau_d$ , anomaly parameter  $\alpha$ . We were able to fit the data with a single component fit and with  $\alpha$  values ranging between  $1.0 \pm 0.2$

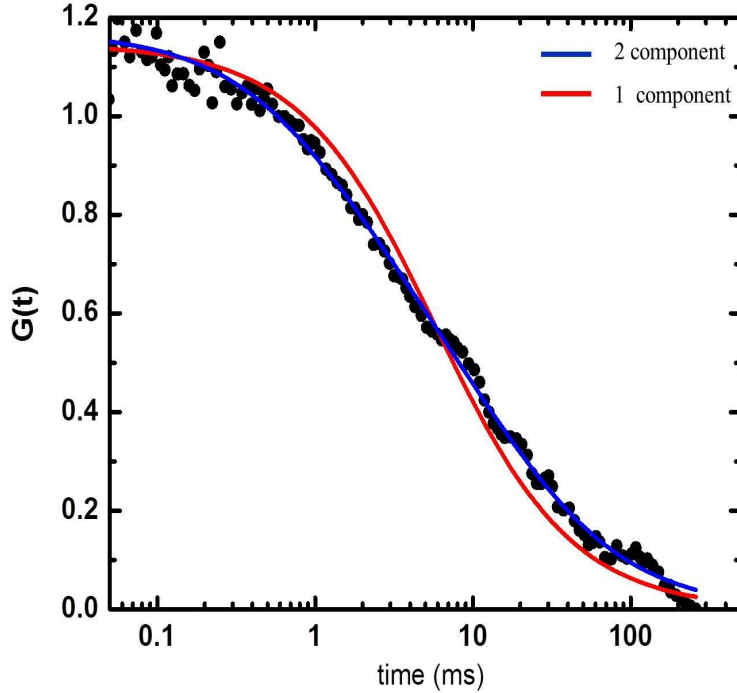


Figure S5: Comparison of fitting done on a QD correlation data using one component and two component model

Laser probe extends axially about  $1.5 \mu m$  and naturally also captures the unbound QD population moving in the bulk. We have contribution of both bound and free QD diffusion. Its diffusion in bulk is always the same irrespective of the underlying bilayer and so we fixed that component during fitting and pulled out only the membrane bound QD diffusion. Transit times shows prominent differences depending on the phase. However, on converting it to diffusion values, this shrinks to a narrow difference due to larger  $\tau_d$  values.

## Kinetics of membrane re - arrangement

As discussed in the main text, there is presence of membrane re - organization on QD addition. This phenomena is reflected in the way  $\tau$  changes with time. Boltzmann - sigmoid fit (Eqn 4 ) is used in extracting relevant time scales of lipid re- arrangement. Figure S6 shows a representative data where this fit is employed and extracted parameters are indicated.

$$y = y_{min} + \frac{y_{max} - y_{min}}{1 + \exp(\frac{t-t_c}{t_R})}, \quad (4)$$

where  $y_{min}$  - initial value,  $y_{max}$  - final value,  $t_c$  - center and  $t_R$  - time constant (rise time).

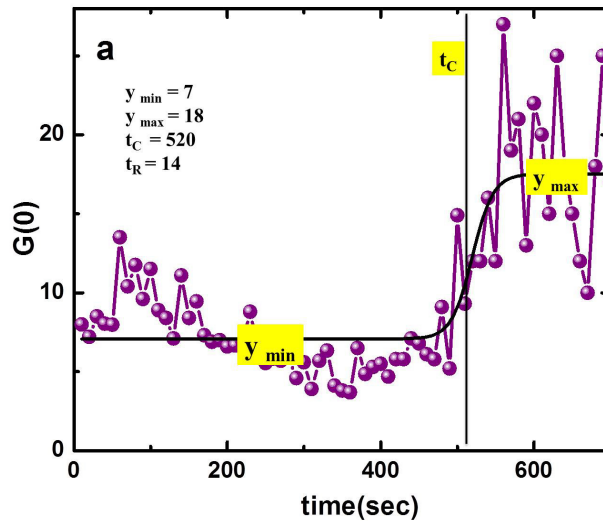


Figure S6: Time dependent changes in  $G(0)$  measured from QD signal at 20um above the bilayer plane. With time,  $G(0)$  increases and saturates indicating that the number of QD in that plane reduced as they start to bind to the membrane (at 0  $\mu m$ ). Solid black line denotes the Boltzmann sigmoid growth fit and corresponding fit parameters are marked in the figure

## Concentration dependent fluidization:

Our results shows that with cationic QDs, DLPC membrane is fluidized. On increasing the concentration of QD,  $\rho$  also increases and corresponding morphology changes drastically with concentration. There is a critical concentration of QD required to see any changes in membrane fluidity. For example, at 0.1nM, membrane shows no changes in its dynamics.

With changes in the amount of QD introduced, membrane fluidity changes accordingly. At 4nM, it gets fluidized 3.5 times and for 1nM this reduces to 2 times as shown in Table S1.

Table S1: Lipid diffusion  $D$

Concentration	$D_{before}(\mu m^2/s)$	$D_{after}(\mu m^2/s)$	Ratio ( $\rho$ )
4nM	$1.8 \pm 0.2$	$6.2 \pm 0.4$	3.5
1nM	$1.7 \pm 0.28$	$3.8 \pm 0.35$	2.2
0.1nM	$1.5 \pm 0.3$	$1.5 \pm 0.4$	1.0

$D_{before}$  and  $D_{after}$  are diffusion values measured before and after QD addition.

## Structural Characterization

### Confocal imaging

Figure S7 shows confocal images of tagged SLBs, where homogeneous bilayer in case of L1P0 and micron scale phase separated domains in case of L1P1 are obtained. We have tagged the bilayer using ATTO 488 DMPE dye and observed that this dye preferentially partitions towards the S phase of L1P1 bilayer. Based on confocal and AFM imaging, we have identified the phases in case of L1P1 bilayer.

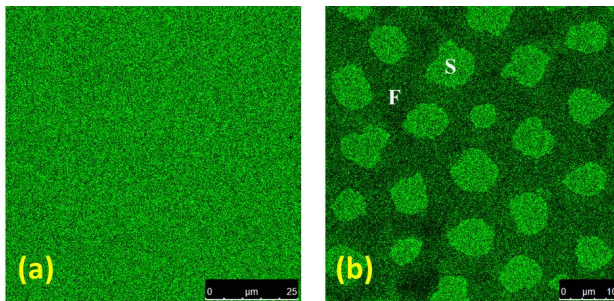


Figure S7: Confocal images of pristine bilayers of a) L1P0, b) L1P1 bilayers tagged with ATTO 488 DMPE dye.

## AFM imaging

AFM imaging of SLBs were performed under liquid using NX100 (Park System, Korea) with a Pyrex-Nitride-Probes-Silicon Nitride (PNP-SiN) cantilever of force constant  $\sim 0.08 Nm^{-1}$ . We used contact mode imaging with a set point of  $0.15 nN$ , scan speed of  $0.5 Hz$  for  $10 \mu m \times 10 \mu m$  using  $50 \mu m^2$  scan head. Images were captured before and after QD addition.

Surface sensitive techniques like AFM and XRR provides useful topographic information and planar supported bilayer platforms are the ideal ones for such studies. Figure S8 and S9 shows the AFM images obtained from different bilayers and height profiles of bilayers before and after addition of QDs in the membrane. In case of L1P0 and L0P1, we obtain a homogeneous bilayer and in case of L1P1, micron scale phase segregated domains with a step height of  $\sim 1nm$  is obtained. On addition of QD, by analyzing the topographic height profiles, we obtain the information on protrusion of QDs outside the membrane. AFM measures site specific changes in the membrane and is sensitive to the phases in case of L1P1. Penetration depth of QD depends on the phase of the membrane underneath and is as follows :  $DLPC \sim L1P1 F > L1P1 S > DPPC$ .

## Xray - reflectivity (XR):

XR gives averaged out sample information on thickness, electron density and roughness before and after QD incubation. This data was collected in BL 18 beamline, Photon Factory, Japan. Igor fit was used in reflectivity fitting of XR data. XR gives averaged out sample information on thickness, electron density and roughness before and after QD incubation. Fitting of reflectivity data<sup>2,3</sup> is shown in Figure S10a for DPPC bilayer, before and after QD incubation and their respective SLD profiles are shown in Figure S10b. Summary of the fits for all the bilayers investigated are given in Figure S11. Before QD incubation, thickness of membrane varies as  $DLPC < L1P1 < DMPC < DPPC$ . On addition of QD, a layer of QD is modeled on top of the membrane with varying thickness. More stiffer the membrane, thickness of QD layer increases. One monolayer thick ( $\sim 9.8nm$ ) QD layer is used to fit

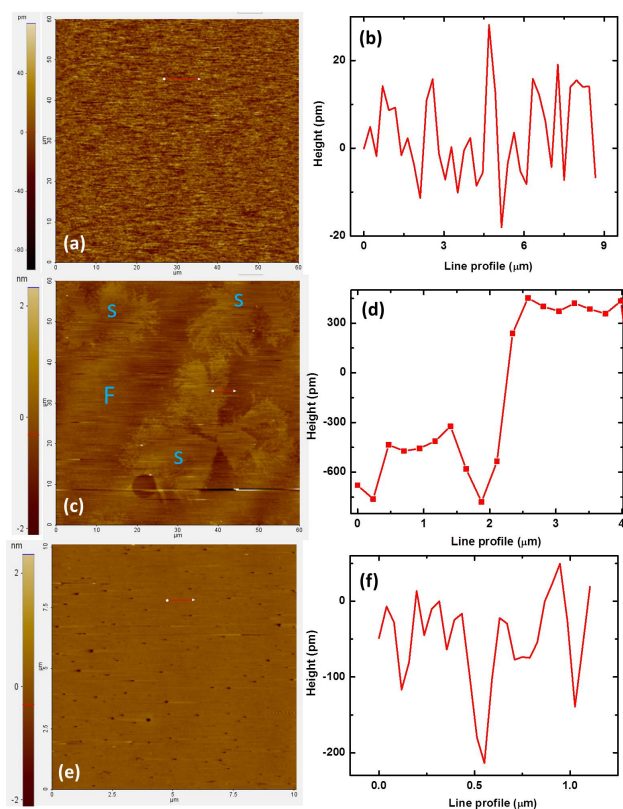


Figure S8: AFM images before addition of QD and corresponding line profiles of a, b) L1P0, c,d) L1P1, e,f) L0P1. Red lines in the images correspond to the line profiles adjacent to the images.

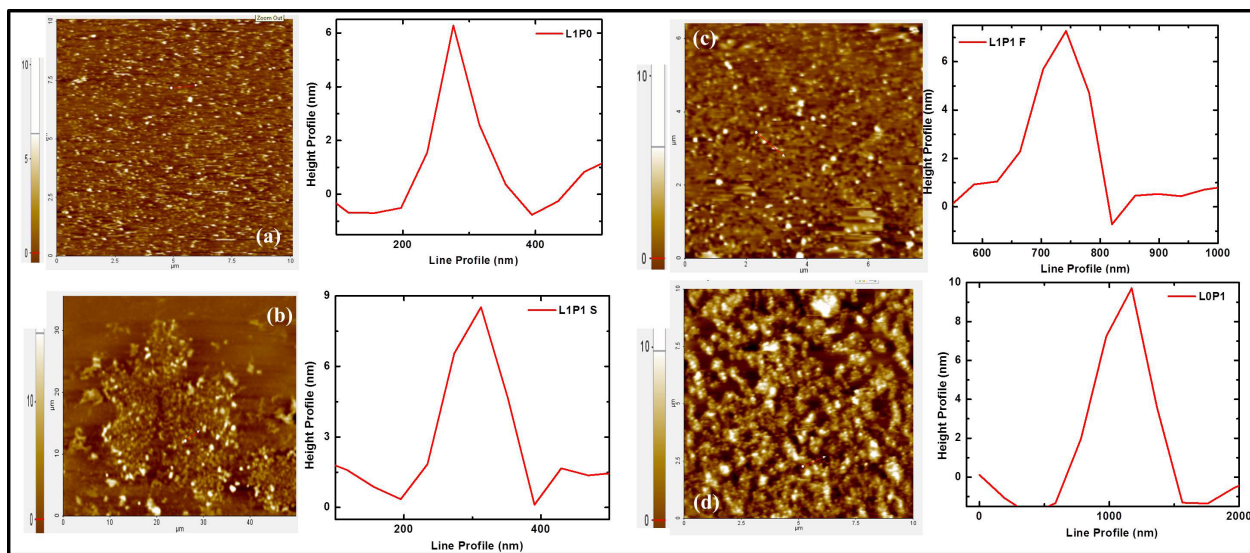


Figure S9: AFM images after addition of QD on a) L1P0, b) L1P1 S, c) L1P1 F and d) L0P1. Red lines in the images correspond to the line profiles adjacent to the images.

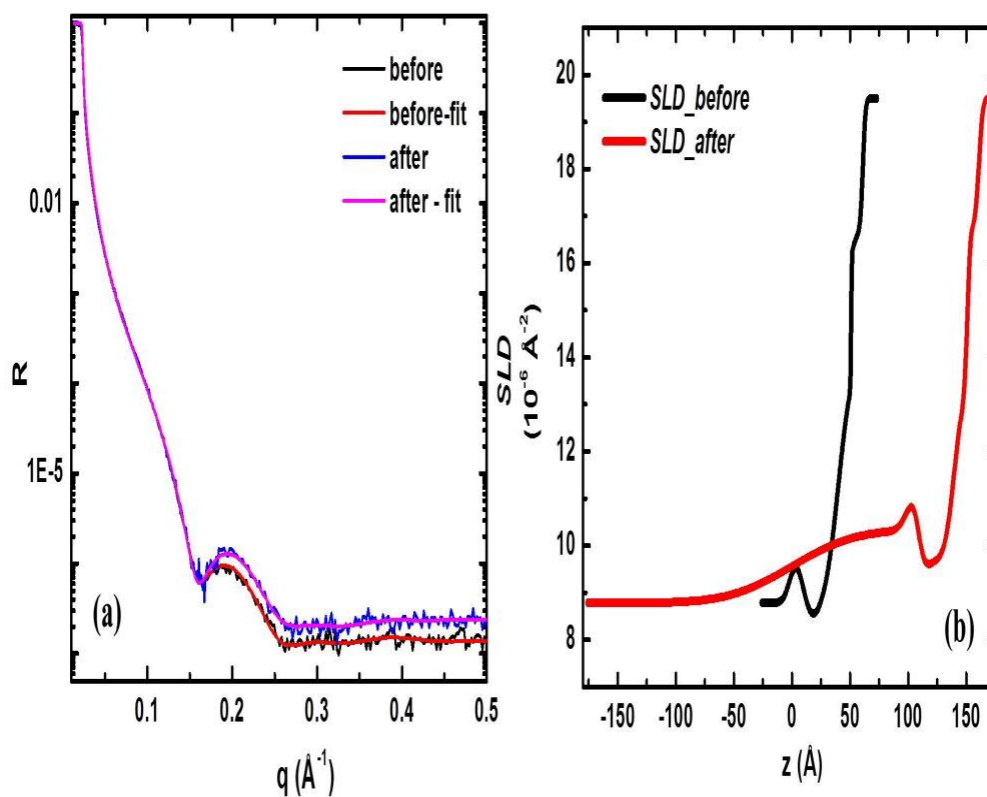


Figure S10: a) Reflectivity profiles of DPPC bilayer obtained before and after QD incubation with respective fits and corresponding b) Scattering length density (SLD) extracted from the fits .

SAMPLE	DLPC		LIP1		DPPC		DMPC	
	d	SLD	d	SLD	d	SLD	d	SLD
<b>Fronting_H20</b>	INF	10	INF	10	INF	10	INF	10
<b>QD</b>	-	-	-	-	-	-	-	-
<b>Head</b>	5.2	14.4	5.7	13.8	9.2	12.4	7.7	15.4
<b>Tail</b>	11.87	7.4	10.15	9.86	13.2	8.52	13.4	7.8
<b>Tail</b>	13.9	8.4	16.2	10.9	19.69	10.5	16	9.1
<b>Head</b>	7.96	16.6	9.9	17.7	10.8	14.87	9.3	16.2
<b>SiO2</b>	10.15	18.6	10.15	18.6	10.15	18.6	10.15	18.6
<b>Backing-Si</b>	INF	20.7	INF	20.7	INF	20.7	INF	20.7

After QD incubation:

SAMPLE	DLPC		LIP1		DPPC		DMPC	
	d	SLD	d	SLD	d	SLD	d	SLD
<b>Fronting_H20</b>	INF	10	INF	10	INF	10.05	INF	10
<b>QD</b>	<u>62.3</u>	11	<u>91</u>	12.3	<u>98.83</u>	11.04	<u>78.6</u>	12
<b>Head</b>	5.1	15.5	5.9	14.3	6.3	15	8.4	15.7
<b>Tail</b>	11.5	8.98	11.85	9.9	12.1	8.9	14.2	8.2
<b>Tail</b>	13.9	9.6	17.7	10.9	19.69	10.5	16.1	10.1
<b>Head</b>	8.1	16.5	9.9	18.0	10.8	14.8	9.3	16.6
<b>SiO2</b>	10.15	18.6	10.15	18.6	10.15	18.6	10.15	18.6
<b>Backing-Si</b>	INF	20.7	INF	20.7	INF	20.7	INF	20.7

Figure S11: XR fitting parameters before and after QD incubation is summarized in the table. Numbers marked in red and underlined corresponds to the thickness of QD layer used in fitting the data

the DPPC data compared to a 6.0 nm thick layer in DLPC membrane. Depending on the penetration of QD, electron density of the lipid layers was also found to get altered.

## Membrane viscosity calculations

Based on the QD diffusion and binding data, we used this information to extract  $\eta_m$ . Different models used in calculating membrane viscosity is discussed below. Summary of values obtained from this calculations are listed in the Table S2 .

### Model 1 :

Saffman - Delbruck (SD) model<sup>4</sup> given by,

$$D = \frac{K_B T}{4\pi\mu_m h} \left( \ln\left(\frac{\mu_m h}{\mu_w r}\right) - 0.58 \right), \quad (5)$$

where  $K_B$  - Boltzmann constant, T - Temperature,  $\mu_m$  - membrane fluid viscosity (Pa.s),  $\mu_w$  - bulk water viscosity (0.0011 Pa.S), h - membrane thickness and r - radius of diffusing molecule (0.5 nm for PC lipids and 5 nm for QDs). It is common in literature<sup>5,6</sup> to represent 2D membrane viscosity in Pa.s.m,

$$\eta_m = \mu_m * h$$

### Model 2 :

DADL (Danov - Aust - Durst - Lange)<sup>7</sup> model has been earlier used for studying diffusion of spherical particles, size of few hundreds of nanometer, unlike SD model (where size should be comparable to that of bilayer thickness 5nm). It is given by,

$$D = \frac{K_B T}{6\pi\eta_w r + \sigma r^{0.1}}, \quad (6)$$

$$\sigma = 8\pi\eta_w(0.22(\frac{2\eta_w}{\eta_m})^{-0.9}) \quad (7)$$

$K_B$  - Boltzmann constant,  $T$  - Temperature,  $\eta_w$  - bulk viscosity of water,  $r$  - radius of molecule,  $\eta_m$  - 2D membrane viscosity

### Model 3 : Fischer's model

Fischer model<sup>8</sup> accommodates for the penetration depth of the particle in mono layer and membrane. At large Boussinesq number(B),

$$D = \frac{K_B T}{4\pi\eta_w r \frac{B}{\ln \frac{B}{\sin\theta}} - \gamma}, \quad (8)$$

where  $\gamma$  - Euler constant,  $\theta$  - contact angle between the interface and QD calculated from the geometrical consideration.  $\theta$  is estimated from protrusion height ( $d$ ) and QD radius ( $r$ ),

$$\frac{\theta}{2} = \tan^{-1} \frac{d}{r} \quad (9)$$

Table S2: Membrane viscosity calculated from Lipid & QD diffusion

SAMPLE	$\eta_{SD}^1$ x $10^{-9}$	$\eta_{SD}^2$ x $10^{-9}$	$\eta_{DADL}$ x $10^{-9}$	$\eta_{Fischer}$ x $10^{-9}$
L1P0	0.6	8.5	8.5	14
L1P1 F	0.85	5.1	5.2	8.5
L1P1 S	1.65	4.5	4.7	7.7
L0P1	-	6.2	6.4	10

$\eta_{SD}^1, \eta_{SD}^2$  - Membrane viscosity calculated from lipid and QD diffusion using SD model.  
 $\eta_{DADL}, \eta_{Fischer}$  - Membrane viscosity calculated from QD diffusion using DADL and Fischer model respectively. Unit of membrane viscosity is given in Pa.s.m

Reported values for fluid bilayers in model membranes using different measurement techniques is in the range of  $10^{-9} - 10^{-10} Pa.s.m.$ <sup>5,6,9</sup> Calculation using lipid D shows an order of magnitude difference compared to the QD D, as continuum hydrodynamic theory fails

at the length scales of lipid. Even though,  $\eta$  estimates lies in this expected range,  $\eta$  of L1P0 is always the largest of all the 3 membrane cases. This is however unexpected from that of a fluid bilayer. Parameters that are considered to influence the molecule diffusion is its size and membrane viscosity. However, Fischer model indicated the significance of ***penetration depth*** of molecule inside the membrane. In a membrane, they inferred that the drag experienced by the particle is maximum when half inserted and drops above or below this condition. Changes in penetration of QD is depicted in the following figure (Figure S12)

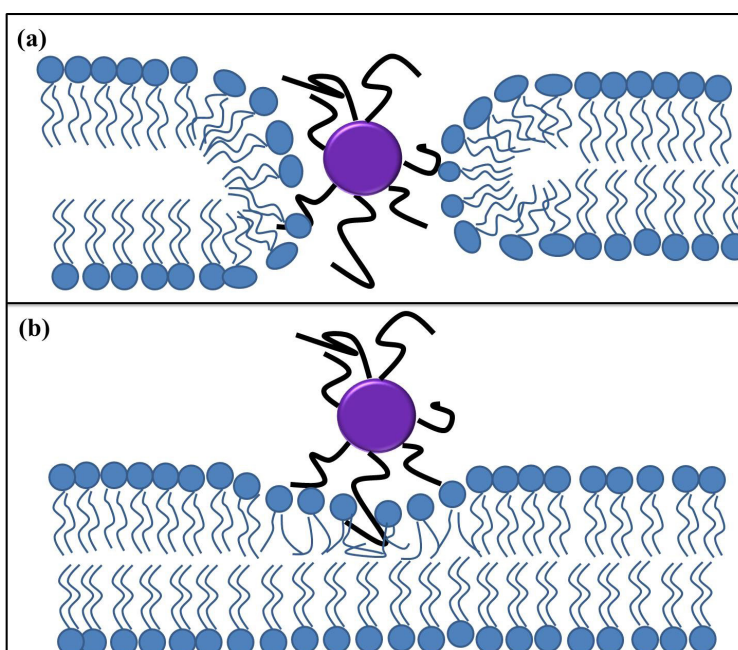


Figure S12: Schematics showing penetration of QD a) Filling the whole bilayer thickness (DLPC , L1P1 F) and b) Partially the monolayer thickness only ( L1P1 S , DPPC)

## References

- (1) Marsh, D. Comment on interpretation of mechanochemical properties of lipid bilayer vesicles from the equation of state or pressure-area measurement of the monolayer at the air-water or oil-water interface. *Langmuir*. **2006**, *22*, 2916.
- (2) Biswas, N.; Bhattacharya, R.; Saha, A.; Jana, N. R.; Basu, J. K. Interplay of electrostat-

- ics and lipid packing determines the binding of charged polymer coated nanoparticles to model membranes. *Phys. Chem. Chem. Phys.* **2015**, *17*, 24238–24247.
- (3) Basu, J. K. Grazing incidence X-ray scattering and diffraction. *Resonance*. **2014**, *19*, 1158–1176.
- (4) Saffman, P.; Delbrück, M. Brownian motion in biological membranes. *Proc. Natl. Acad. Sci. U.S.A.* **1975**, *72*, 3111–3113.
- (5) Honerkamp-Smith, A. R.; Machta, B. B.; Keller, S. L. Experimental observations of dynamic critical phenomena in a lipid membrane. *Phys. Rev. Lett.* **2012**, *108*, 265702.
- (6) Hormel, T. T.; Kurihara, S. Q.; Brennan, M. K.; Wozniak, M. C.; Parthasarathy, R. Measuring lipid membrane viscosity using rotational and translational probe diffusion. *Phys. Rev. Lett.* **2014**, *112*, 188101.
- (7) Shigyou, K.; Nagai, K. H.; Hamada, T. Lateral Diffusion of a Submicrometer Particle on a Lipid Bilayer Membrane. *Langmuir*. **2016**, *32*, 13771–13777.
- (8) Fischer, T. M.; Dhar, P.; Heinig, P. The viscous drag of spheres and filaments moving in membranes or monolayers. *J. Fluid Mech.* **2006**, *558*, 451–475.
- (9) Stanich, C. A.; Honerkamp-Smith, A. R.; Putzel, G. G.; Warth, C. S.; Lamprecht, A. K.; Mandal, P.; Mann, E.; Hua, T.-A. D.; Keller, S. L. Coarsening dynamics of domains in lipid membranes. *Biophys. J* **2013**, *105*, 444–454.